IOP Publishing Journal of Optics
J. Opt. **16** (2014) 105012 (10pp) doi:10.1088/2040-8978/16/10/105012

Effective non-retarded method as a tool for the design of tunable nanoparticle composite absorbers

Guillermo Ortiz[1], Marina Inchaussandague[2], Diana Skigin[2], Ricardo Depine[2] and W Luis Mochán[3]

[1] Departamento de Física, Facultad de Ciencias Exactas, Naturales y Agrimensura, Universidad Nacional del Nordeste, Avenida Libertad 5470, W3404AAS Corrientes, Argentina
[2] Grupo de Electromagnetismo Aplicado, Departamento de Física, FCEN, UBA and IFIBA, CONICET, Pabellón 1, Ciudad Universitaria, 1428 Buenos Aires, Argentina
[3] Instituto de Ciencias Físicas, Universidad Nacional Autónoma de México, Apartado Postal 48-3, 62251 Cuernavaca, Morelos, México

E-mail: gortiz@unne.edu.ar

Received 19 June 2014, revised 7 August 2014
Accepted for publication 8 August 2014
Published 23 September 2014

Abstract

We investigate the capabilities of an effective non-retarded formalism (ENR) for the exploration and design of nanoparticle composites with specific optical properties. We consider a composite material comprising periodically distributed metallic spheres in a dielectric host matrix. The effective macroscopic dielectric function of the composite medium is obtained by means of the ENR and is used to calculate the electromagnetic response of a slab made of an inhomogeneous material. This response is compared with that obtained by using the layer Korringa–Kohn–Rostoker wave calculation method (LKKR). We analyze the optical properties for different filling fractions, especially in the vicinity of the resonance frequencies of the macroscopic dielectric function. We notice that for dense systems within the long wavelength regime, the results of some analytical theories developed by other authors do not properly describe the multipolar excitations and interactions of orders higher than the dipole, in contrast with the results obtained by using an ENR. Therefore, those methods are not suitable for the design of compound films with novel properties. We show that by appropriately choosing the parameters of the composite, it is possible to achieve a tunable absorber film, and more generally, we show that ENR is a versatile tool for the design of nanoparticle composite materials with specific properties.

Keywords: effective media, optical resonances, recursive methods, thin films, tunable absorbers, nanoparticles
PACS numbers: 78.67.Bf, 77.22.Ch, 78.20.Ci, 78.20.Bh

(Some figures may appear in colour only in the online journal)

1. Introduction

The optical properties of inhomogeneous materials have been extensively studied for several decades. Some formalisms, such as the theories of spectral representations [1–3], spatial fluctuations [4, 5], renormalized polarizabilities [6, 7], and diagrammatic series [8, 9], attempt to obtain the electromagnetic macroscopic response of these systems by using analytical and/or semi-analytical expressions. If the typical wavelengths are much larger than the size of the inhomogeneities, it is possible to design a quasi-static treatment (also called long wavelength approximation) that is the basis for many of the current methods for determining the effective electric macroscopic permittivity of the system. An enlightening review of traditional approaches to solving the problem

by means of effective medium models can be found in several studies [10–13].

We are interested in ordered inhomogeneous systems formed by two phases, one metallic and the other dielectric. Our interest in metal–dielectric composites lies in the possibility of designing their optical properties by adapting the parameters of the materials. More specifically, if the phases of the composite are chosen with appropriate geometry and sizes, it is possible to tune the resonance of the dielectric macroscopic function within the visible range [14–17]. Effective medium theories describe the macroscopic dielectric function of complex composite nanostructures in terms of the dielectric functions of their components and of a limited number of geometrical parameters. In the case of diluted systems with spherical inclusions, the filling fraction is sufficient information to obtain the macroscopic dielectric function, as established by the traditional effective medium theories [18, 19], in which only dipolar contributions among the particles that compose the system are taken into account. However, most of the interesting effects are more strongly manifested for inclusions with complex geometries and close to the percolation threshold of the conductive phase—i.e., in systems with high filling fractions.

Waterman *et al* [20] proposed an expansion of the macroscopic dielectric function in terms of the filling fraction of an infinite periodic array of spheres. It is well known that for high concentrations of metallic particles, the multipolar interactions yield a macroscopic dielectric response that exhibits higher-order resonances, independently of the size of the particles [21, 22]. Although Waterman's formulation takes into account the multipolar interactions between the scatterers, the predicted contribution of these higher-order terms is almost negligible. Therefore, many later works have stated that the corrections to the Maxwell Garnett formulation that account for higher-order multipolar effects would be significant *only* for systems with large particles compared with the operating wavelength, i.e., beyond the long wavelength limit, and would be negligible for small particles even in the case of a large filling fraction. This situation prompted the development of the Extended Maxwell Garnett approximation, which has been employed by many authors [23–25]. Among the theories developed to study non-diluted [26, 27] and ordered [14, 22, 28] systems, the effective non-retarded method (ENR) has been recently proposed. This formalism makes it possible to obtain the complex and frequency dependent macroscopic dielectric function for arbitrarily shaped inclusions, either particles or vesicles, periodically ordered in 2D or 3D arrays. It can also deal with interpenetrating inclusions and dissipative and dispersive materials [15]. Although the ENR allows dealing in principle with inclusions of arbitrary geometry, it seems to be better suited for particles or vesicles with planar faces, such as cubes or parallelepipeds. This is because its numerical implementation requires a discrete representation; a cubic grid is used to discretize the unit cell.

Given the demonstrated versatility of this method for predicting the optical properties of complex materials [16], it is important to assess its behavior when applied to the case of composites with curved surfaces, such as those made of spherical inclusions, like those that have been recently manufactured [29–31]. The case of spherical inclusions requires a detailed analysis of the numerical procedure employed to determine the dielectric macroscopic function. Moreover, it is essential to validate the results by comparison with rigorous methods which do not include approximations in the representation of the shape of the inclusions. Among these methods, the layer Korringa-Kohn-Rostoker (LKKR) makes it possible to investigate the electromagnetic response of composites formed by periodic arrays of spheres and has been shown to be numerically efficient. In the LKKR, the electromagnetic interactions between the scatterers are calculated by means of the layer-multiple-scattering method for spherical particles [32–35]. Recently, simulated reflectance spectra calculated by means of the vector LKKR at high-order band frequencies have shown a clear correlation between theoretical and experimental results [36].

The main advantage of the ENR over the LKKR is the possibility of studying the optical properties of composites with arbitrary geometries, including systems formed by dielectric vesicles within a conducting medium and interpenetrated systems [15–17]. We will show that the ENR is applicable to the case of spherical metallic composites embedded in a dielectric medium and that it can satisfactorily predict multipolar effects of higher-order. To do so, we investigate the electromagnetic response of a composite slab and compare the results obtained by using the ENR and the LKKR. In section 2, we use the ENR to obtain the macroscopic dielectric response of a medium comprising a simple cubic lattice of spheres. In section 3, we use the LKKR to obtain the electromagnetic response of a composite material slab and is compared with that given by the ENR. In section 4 we explore the potential of the ENR as a design tool for tunable absorbers from diluted to overlapping particles. Finally, we provide concluding remarks in section 5.

2. The macroscopic dielectric function

Let us consider a composite made up of arbitrarily shaped inclusions arranged in a periodic 3D array. Provided that the length of the inclusions in the material is small compared with the electromagnetic wavelength, this mixture can be treated as a homogenized composite material. The ENR method is based on Haydock's recursive scheme [37], from which a tridiagonal representation of a characteristic function [15, 16] is obtained and yields the macroscopic dielectric function (ϵ^M) of the composite. This result depends on the shape of the inclusions, on the dielectric function of the components, and on the filling fraction (f) of the array (the ratio of the volume occupied by particles in the unit cell to the total volume of the unit cell). Since the coefficients that appear in the tridiagonal representation depend on the shape of the particles and on f, but *not* on the dielectric constant of the inclusions, once they are obtained for a particular geometry and concentration

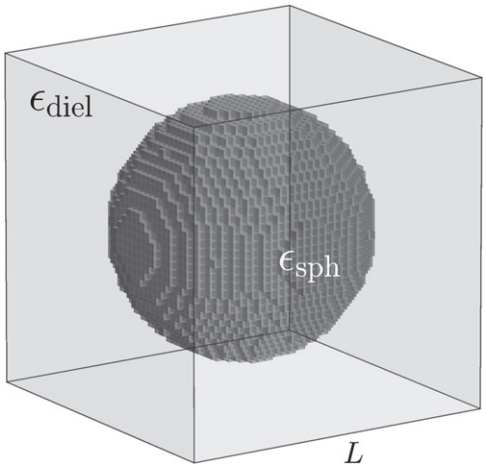

Figure 1. Unit cell of a simple cubic lattice of lattice parameter L made up of spherical particles of radius r and dielectric function ϵ_{sph} embedded in a matrix with dielectric constant ϵ_{diel}. The sphere is discretized by small cubes of side $L/(2\,M+1)$. In this illustration, $r = 0.38L$ and $M = 20$).

of the scatterers they can be used for inclusions of different materials, saving considerable computation time.

In the following discussion, we apply the ENR to investigate materials with spherical inclusions arranged in a simple cubic lattice of period L (figure 1). We consider an array of metallic spheres embedded in a dielectric host material of permittivity ϵ_{diel}. To model the permittivity of the metal ϵ_{sph} as a function of frequency ω, we use the Drude formula

$$\epsilon_{\text{sph}}(\omega) = 1 - \frac{\omega_p^2}{\omega^2 + i\,\omega\,\Gamma}, \tag{1}$$

where ω_p is the bulk plasma frequency, Γ stands for the relaxation time, and i is the imaginary unit.

For the numerical implementation, the unit cell is divided into $(2M+1)^3$ cubes of side $L/(2M+1)$ by taking $2M+1$ equidistant points on each of its sides, and the discretized inclusion is defined by the set of cubes contained within the volume of the actual sphere. The discretization process is particularly suitable for particles with planar facets, since they can be exactly represented by stacking cubes. For curved inclusions, the discretized particle exhibits a stepped surface (as shown in figure 1 for $M = 20$) that becomes smoother as M increases. The choice of M is not only important to properly represent the geometry of the particle but also to obtain an acceptable resolution in the Fourier transform calculations involved in the ENR [15]. The appropriate value for M must be found for each combination of parameters. We implemented the ENR by using the Perl Data Language [38].

In figure 2 we show the real and imaginary parts of the macroscopic dielectric function as a function of the photon energy $\hbar\omega$ within the optical range for $M = 60$ and 120. We consider two different composites: (a) one made of silver (Ag) particles ($\hbar\Gamma = 0.03$ eV and $\hbar\omega_p = 8.5$ eV) embedded in a titanium dioxide (TiO_2) matrix ($\epsilon_{\text{diel}} = 7.84$), and (b) the other made of gold (Au) particles ($\hbar\Gamma = 0.1$ eV and $\hbar\omega_p = 7.0$ eV) immersed in a tellurium dioxide (TeO_2) matrix ($\epsilon_{\text{diel}} = 5.2$). The parameters $\hbar\omega_{\text{p}}$ and $\hbar\Gamma$ were obtained by fitting the real and imaginary parts of the dielectric function given by (1) to the experimental data of [39] in the NIR-VIS range; this fit is adequate below 3 eV. Two different filling fractions are considered in both cases: $f = 0.045$ ($r = 0.22\,L$, left panels) and $f = 0.23$ ($r = 0.38\,L$, right panels).

In figure 2, we also include results obtained from the Waterman formulation (W), which coincide with those obtained by the Maxwell–Garnett approach (MG) and by the Extended Maxwell-Garnett formula [23–25] (not shown), as expected by the long wavelength approximation. As shown in figure 2(a), the curves exhibit a sort of ripple that smooths out as M is increased. This fluctuation is more significant for the composite of Ag spheres than for that of Au spheres (figure 2(b)), suggesting that the choice of a proper value of M is more critical when the contrast between the permittivities of the constituent materials is higher and also for smaller values of Γ. Since the memory requirements for computing the coefficients of the tridiagonal representation of the characteristic function of the composite increase with $(2M+1)^3$, in what follows we have chosen $M = 120$, which yields an adequate convergence. We can estimate the error due to this finite discretization through its effect on the first Haydock coefficient, which is given by the average of the characteristic function within the unit cell [16] and which should thus converge towards f as M increases. Taking $M = 120$, the relative error of this coefficient is $\approx 0.04\%$ for $f = 0.045$, and it decreases as f increases.

From the Mie theory, an isolated sphere is expected to exhibit multipolar resonances for $\epsilon_{\text{sph}} = -\epsilon_{\text{diel}}(l+1)/l$, where l is a positive integer [40], with corresponding frequencies

$$\omega \approx \sqrt{\omega_p^2/\left(1 + \epsilon_{\text{diel}}(l+1)/l\right)}, \tag{2}$$

according to equation (1). The dipole resonance ($l = 1$) is at $\hbar\omega \approx 2.1$ eV for both compositions considered above. As could be expected, for our dilute $f = 0.045$ composites, Im $\{\epsilon^M\}$ exhibits a peak close to this isolated dipolar resonance. However, for our dense $f = 0.23$ system, the multiple scattering between the spheres has a significant impact on the optical response of the system; consequently, the resonant frequency is red-shifted towards $\approx$1.71 eV. In this case, Im $\{\epsilon^M\}$ exhibits a second peak at ≈ 2.5 eV which is associated with an octupole resonance ($l = 3$ in equation (2)) [22]. Notice that only resonances with odd l can be excited due to the symmetry of the system. Surprisingly, this peak does not appear in the Waterman results, although his approach takes into account higher-order interactions between the scatterers. For the diluted case, the overall matching of the ENR and the W curves is very good. However, the dipole resonance peak obtained by the ENR is lower and slightly wider than that predicted by the W. This may be due to the discretized nature of the spherical particle within the ENR. In all cases, Re $\{\epsilon^M\}$

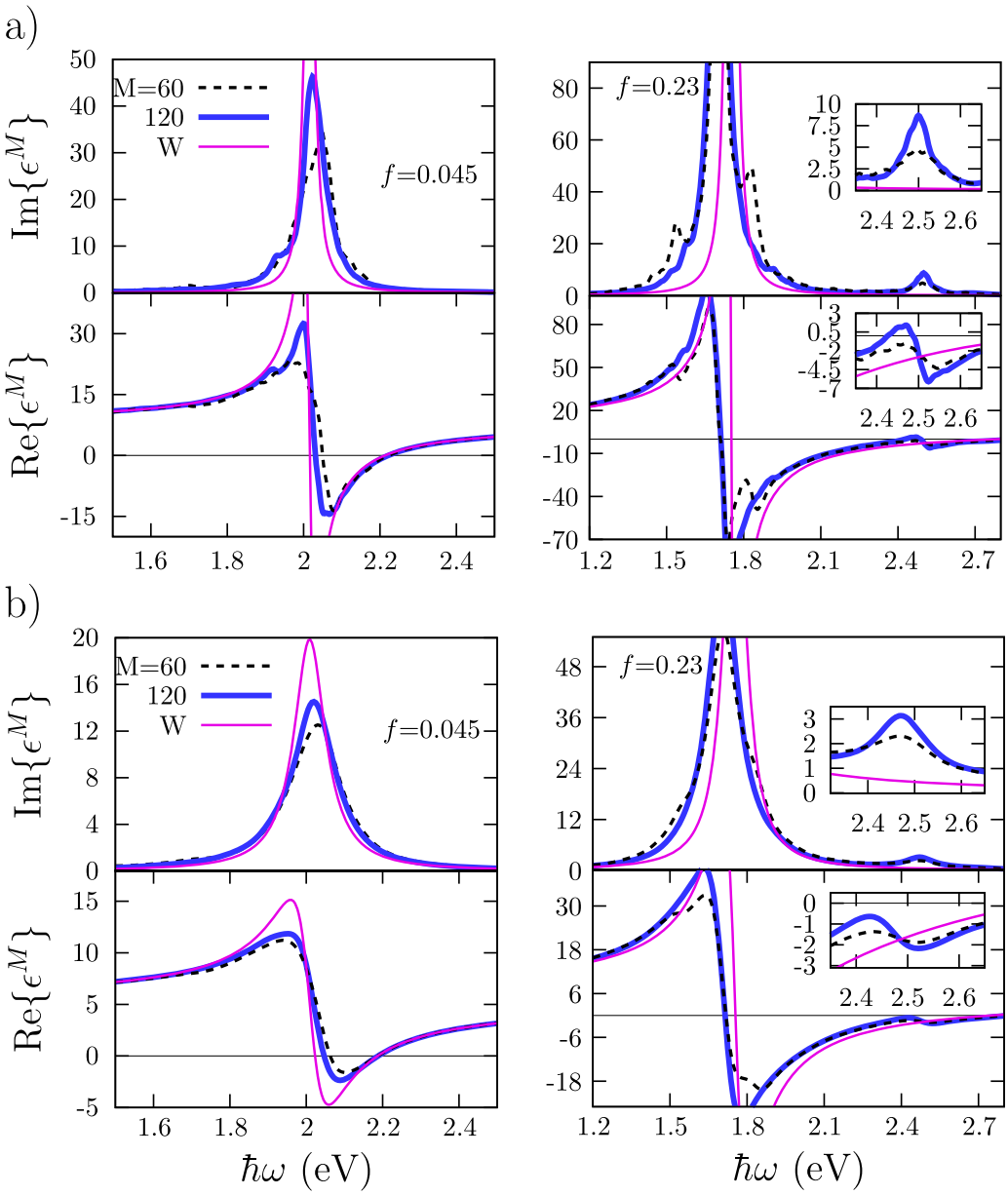

Figure 2. Imaginary and real parts of the macroscopic dielectric function ϵ^M of a simple cubic lattice of metallic spheres embedded in a dielectric matrix: (a) Ag spheres within TiO_2, (b) Au spheres within TeO_2. The left side corresponds to $f = 0.045$ and the right side to $f = 0.23$. Dashed lines and thick solid lines correspond to $M = 60$ and 120, respectively. For $f = 0.23$, the insets show the vicinity of $\hbar\omega \approx 2.5$ eV. Results given by the Waterman *et al* model (W) are shown as thin solid lines.

and Im $\{\epsilon^M\}$ satisfy the Kramers–Kronig relationship, as expected.

3. Optical properties of nanocomposite thin films

In this section, we analyze the electromagnetic response of a slab made of a composite material. We first use the LKKR to investigate the influence of the number of layers of spheres on its optical properties and establish the conditions for which the results given by the LKKR permit a valid comparison with those of the effective medium theory (ENR). In figure 3 we show schematically (a) the composite slab modeled with the LKKR and (b) its view according to the ENR.

3.1. The LKKR method

Among the methods available for the calculation of the electromagnetic response of composite periodic structures made of spheres, the LKKR appears to be numerically efficient. Within its framework, the electromagnetic interactions between the inclusions arranged in the periodic lattice are calculated by means of the layer-multiple scattering method for spherical scatterers [32–35]. The crystal can be considered as a stack of parallel layers formed by spheres periodically arranged in a 2D Bravais lattice. To solve the electromagnetic problem, the multiple scattering between spheres of each single layer is calculated first. Then the scattered response of multiple layers is determined by using a procedure similar to

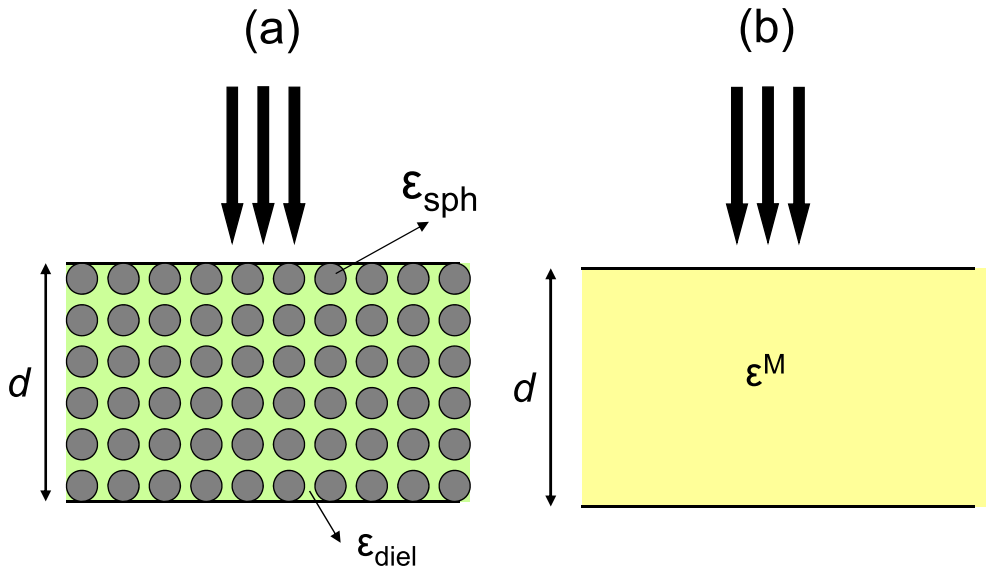

Figure 3. Nanocomposite freestanding film (thickness d). The thick black arrows indicate the propagation direction of the incident field. (a) LKKR: composite slab made of N layers of metallic spheres of permittivity $\epsilon_{\rm sph}$ immersed in a dielectric host medium of permittivity $\epsilon_{\rm diel}$. In the figure, we illustrate the case $N = 6$. (b) ENR: slab of a homogeneous material characterized by the macroscopic dielectric function ϵ^M.

the one used to calculate the reflection and transmission properties of stratified media with planar interfaces. The computer program MULTEM [33, 35] is a numerical implementation of the LKKR.

As mentioned in section 2, the optical response given by the ENR is determined by the filling fraction f of the structure. In contrast, to perform the simulations using MULTEM, the number of layers of spheres within the slab (N) is required. As a consequence, if we fix the thickness (d) of a slab and take the filling fraction of the nanomaterial to be a simple cubic lattice of non-overlapping spheres, the lattice parameter L and the radius r of the spheres are determined by $L = d/N$ and $r = L(3f/4\pi)^{1/3}$. Thus, given d, by varying N, it is possible to find different pairs of values r, L that correspond to the same f.

To investigate the influence of the number of layers for fixed values of d and f, in figure 4 we plot the reflectance R and the absorptance A of a freestanding film made of our Ag/TiO_2 system and illuminated by normally incident light as a function of the photon energy $\hbar\omega$ for $d = 360$ nm and 1820 nm and different values of N, calculated with the LKKR method. For both thicknesses, we consider two different filling fractions, $f = 0.045$ (top panel) and $f = 0.23$ (bottom panel). As N increases, r and L become smaller, the wavelength becomes relatively larger, and thus it is to be expected that the long wavelength condition is asymptotically approached. This behavior can be verified in figure 4, in which the curves for large N are close to each other. In table 1 we summarize the values of L and r for the slabs investigated in the present example. According to the values of r given in table 1, we can conclude that 32 layers for $d = 360$ nm and 128 layers for $d = 1820$ nm are sufficient to ensure the long wavelength condition within the spectral range considered.

3.2. Comparison between the LKKR and the ENR

Figure 5 displays the reflectance, absorptance, and transmittance of the same films as in figure 4 obtained by using three different approaches: LKKR, ENR, and W. For the ENR calculations we used $M = 120$. Taking into account the analysis of section 3.1, for the LKKR simulations we used $N = 32$ for $d = 360$ nm and $N = 128$ for $d = 1820$ nm. The electromagnetic response of the slab is closely linked to the macroscopic dielectric function of the composite, i.e., to the behavior of Re $\{\epsilon^M\}$ and Im $\{\epsilon^M\}$, which are strongly frequency dependent (see figure 2). Accordingly, the response of the slab exhibits different features in different spectral regions.

For low frequencies ($\hbar\omega < 2$ eV for $f = 0.045$ and $\hbar\omega < 1.7$ eV for $f = 0.23$), the curves for both values of f display oscillations due to the Fabry–Perot interference and, as expected, adjacent maxima are closer to each other for thicker slabs. In this spectral region, Re $\{\epsilon^M\} > 0$ (as shown in figure 2 (a)) and therefore the effective medium behaves as a lossy transparent material that allows partial transmission across the slab. However, as the dipole resonance frequency is approached from below, Re $\{\epsilon^M\}$ and Im $\{\epsilon^M\}$ increase, and as a result, a lower transmittance is observed. This behavior becomes more evident for the thicker slab as observed on the right of figure 5 (b), in the ranges $1.8\,{\rm eV} < \hbar\omega < 2\,{\rm eV}$ for $f = 0.045$ and $1.5\,{\rm eV} < \hbar\omega < 1.7\,{\rm eV}$ for $f = 0.23$.

It can be observed that for both thicknesses considered, a high reflectance band starts at the dipole resonance frequency: at ≈2 eV (620 nm) for $f = 0.045$ and at ≈1.7 eV (729.4 nm) for $f = 0.23$ (see left panels of figure 5). Within this band, the reflectance is very high (more than 80%) and the transmittance is negligible. Notice that right at the dipole resonance Re $\{\epsilon^M\}$ changes sign and becomes negative in a frequency

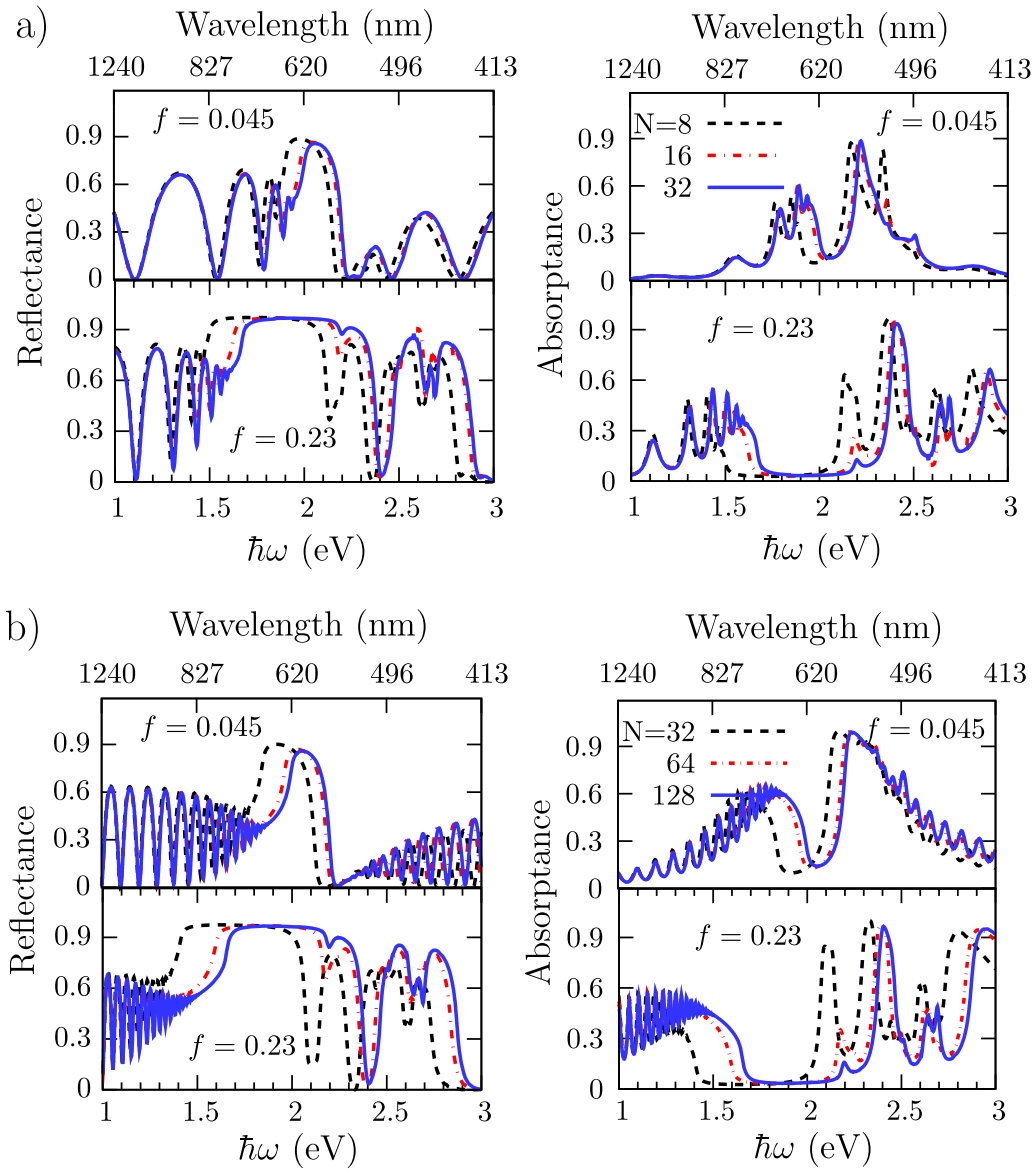

Figure 4. Reflectance R (left) and absorptance A (right) of a composite slab made of Ag spheres embedded in a TiO_2 matrix, as calculated with the LKKR method. (a) d = 360 nm, N= 8, (dashed), 16 (dot-dashed) and 32 (solid). (b) d = 1820, N = 32 (dashed) 64 (dot-dashed) and 128 (solid). Top (bottom) panels in each group correspond to f = 0.045 (f = 0.23).

Table 1. Geometrical parameters of the composite slab considered in figure 4.

d(nm)	N	L(nm)	r(nm) (f = 0.045)	r(nm) (f = 0.23)
	8	45	9.9	17.1
360	16	22.5	4.95	8.55
	32	11.25	2.47	4.27
	32	56.87	12.51	21.61
1820	64	28.44	6.25	10.80
	128	14.22	3.14	5.41

range that defines the reflectance bandwidth. This band is wider for f = 0.23 (1.7 eV < $\hbar\omega$ < 2.9 eV) than for f = 0.045 (2 eV < $\hbar\omega$ < 2.2 eV) because the dipolar interaction is stronger for higher concentrations of spheres, as observed in figure 2(a). Besides, for f = 0.23 there is a pronounced dip within the high reflectance band very close to the octupolar resonance at ≈ 2.5 eV. This dip is located within a narrow frequency range within which Re $\{\epsilon^M\}$ is positive (see figure 2 (a)) and in which the effective medium behaves again as a lossy transparent material which allows light propagation. However, the electromagnetic response in this region differs substantially from that exhibited in the low frequency zone, as in the vicinity of the multipole resonance Re $\{\epsilon^M\} \approx 1$; therefore the contrast between the macroscopic permittivity of the slab and that of the vacuum is very low. Consequently, the reflectance becomes negligible and most of the incident energy enters the slab and is largely absorbed, although in this region Im $\{\epsilon^M\}$ is smaller than at the dipole resonance. A similar effect has already been reported in 2D [14] and 3D structures [16].

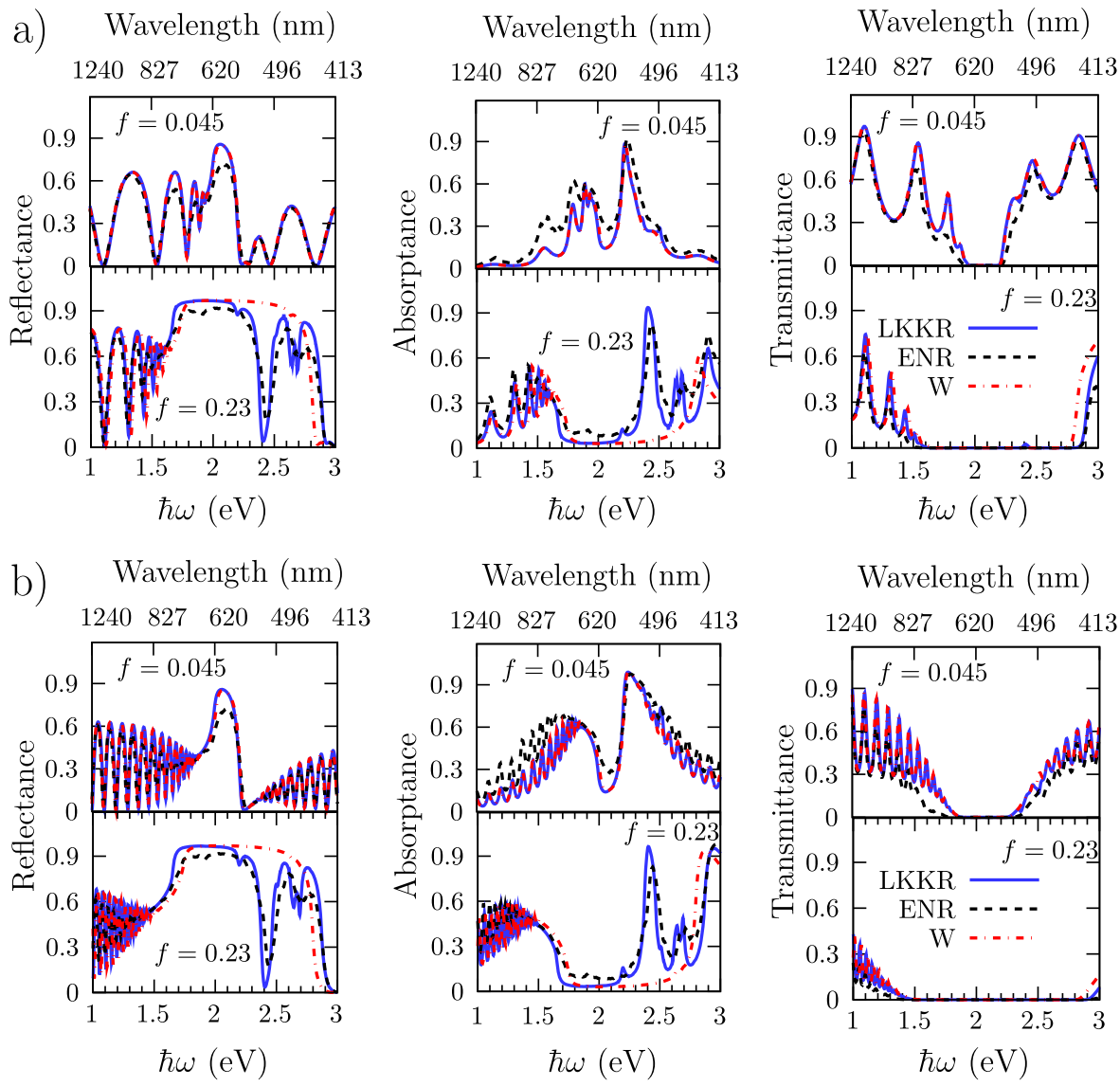

Figure 5. Reflectance R (left), absorptance A (center) and transmittance T (right) of a composite slab made of Ag spheres embedded in a TiO_2 matrix. (a) d = 360 nm and b) d = 1820 nm. Top (bottom) panels of each pair correspond to $f = 0.045$ ($f = 0.23$). We show results of the LKKR (solid), ENR (dashed), and W (dot-dashed) models.

In general, the qualitative agreement between the ENR and the LKKR curves is satisfactory. Both methods adequately describe the spectral response of the composite slab. However, there are some quantitative differences in certain spectral ranges which could be due to the roughness of the discretized spheres in the ENR, which produces modes that affect the electromagnetic response. For $f = 0.045$, the LKKR and W curves are in excellent agreement. However, for $f = 0.23$, the Waterman formulation does not predict the splitting of the reflectance band. Although LKKR, ENR, and W consider in their formulations multipolar interactions between the spheres, only LKKR and ENR adequately describe the splitting of the reflection band at those frequencies at which multipole resonances are excited. From the point of view of potential applications, compound metal–dielectric films can be used as light absorbers [41] the frequency of which may be tuned by appropriately choosing f and ϵ_{diel}.

4. Tuning of absorption bands

In this section we show that by properly combining the filling fraction of the array of nanoparticles and the dielectric constant of the host medium, composite films can be used as tunable frequency light absorbers. Figure 6 displays the absorptance vs. frequency for a composite slab made of Ag spheres embedded in titanium dioxide, as in the previous examples, for different values of f, from $f = 0.05$ (diluted composite of metallic spheres) up to $f = 0.9$ (interpenetrated spheres). The slab is illuminated under normal incidence and its thickness is 1820 nm.

Notice that the reflection band discussed for figure 5 corresponds to a wide flat-bottomed valley in figure 6. Within this band the absorptance $A < 10\%$. As f increases, its spectral position is red-shifted and its bandwidth changes. In contrast, an absorption band for which the absorptance is $A > 90\%$ is located near $\hbar\omega \approx 2.2$ eV (564 nm) for $f \approx 0.05$ and its position

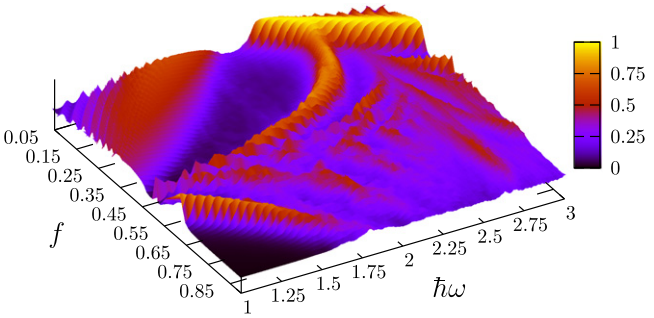

Figure 6. Absorptance of a composite slab of thickness $d = 1820$ nm made of a sc lattice of Ag spheres embedded in TiO_2 as a function of filling fraction f and energy $\hbar\omega$, as calculated with the ENR method.

is blue-shifted as f increases, reaching $\hbar\omega \approx 3$ eV (412 nm) for $f \approx 0.25$. At $f \approx 0.15$ a second absorption peak splits from the main absorption band and is redshifted as f increases up to $f = 0.5$. This peak originates from the octupolar resonance [22]. At $f = \pi/6 \approx 0.52$ the system percolates and becomes conducting. For larger f, the spheres interpenetrate and the interaction among the dielectric interstices produces an absorption band ($A \approx 90\%$) due to the index matching between the macroscopic dielectric function and air at near infrared (NIR) resonant frequencies [14, 16]. As f increases, this band shifts to higher frequencies, as expected. Notice that we took advantage of the computational efficiency and versatility of the ENR method to swiftly and exhaustively explore the parameter space of the system, including regions with non-trivial geometries such as that corresponding to interpenetrated spheres.

So far, we have investigated the absorptance of the slab by considering different filling fractions for a fixed value of the dielectric constant of the host medium. To investigate the influence of ϵ_{diel} in the distribution of the absorption bands, we show in figure 7 the absorptance of a composite slab of Ag nanoparticles as a function of the response of the host ϵ_{diel} for a fixed filling fraction $f = 0.23$. As ϵ_{diel} increases, the dipole and multipole resonances and the corresponding absorption bands are red-shifted, whereas the bandwidths remains approximately constant.

These examples show that the ENR constitutes a useful and powerful tool for the design of tunable absorbers based on metallic nanoparticle composites: by appropriately selecting the filling fraction and the permittivity of the host medium, the electromagnetic response can be tuned to obtain, for example, absorption peaks and negligible transmittance and reflectance in the visible range of the electromagnetic spectrum.

As a final example that further illustrates the versatility of the ENR for attacking more complex geometries, in figure 8 we show the absorptance A of a slab of width $d = 1820$ nm made of a composite composed of Ag square nanoprisms with sides a_x and $a_y = a_z$ along the cartesian axes arranged in a simple cubic lattice with lattice parameter L within a TiO_2 matrix as a function of the aspect ratio $\zeta \equiv a_x/a_y$ and the photon energy $\hbar\omega$ for a fixed filling fraction $f = 0.3$. For definitiveness, we assume the incident light is polarized along the x direction and impinges normally on the slab,

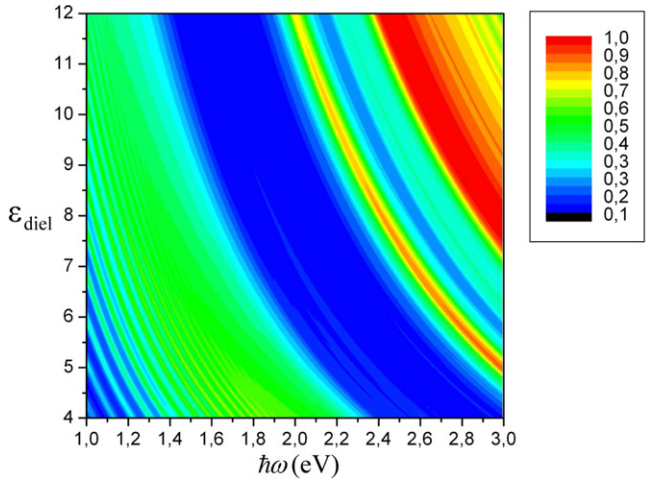

Figure 7. Absorptance of a composite slab made of Ag spheres for $f = 0.23$ versus ϵ_{diel} and $\hbar\omega$.

propagating along the z direction. Notice that for $\zeta = f$ the neighbor prisms coalesce to form a 1D superlattice of continuous conducting planes along the yz directions alternating with dielectric layers. Thus, in this 1D limit the response of the system is given exactly by the 1D Maxwell MG expression, as verified by the figure. In contrast, for $\zeta = 1/\sqrt{f}$, neighbor prisms coalesce to form a square array of wires continuously conducting along the x direction, the response for which should be given exactly by the MG theory in 2D [12], which is again verified by figure 8. In both the 1D and 2D MG theories we take the polarization along the optical axis of the structure. For the intermediate value $\zeta = 1$ the system is given by a cubic lattice of nanocubes, each of which has a several optically active resonances, as described by Fuchs [42], which yield absorption peaks which are shifted due to the interaction among neighbors. These peaks are further shifted as the particles are deformed by changing ζ.

5. Conclusions

We have considered a composite material made up of a periodic lattice of metallic spheres within a dielectric host matrix. The capabilities of the ENR approach in calculating its effective macroscopic dielectric function have been investigated. We have compared the optical response of a composite slab obtained by the ENR with that obtained from the LKKR. We have shown that within the long wavelength regime the two methods agree.

Both methods adequately describe the spectral response of a composite slab. We analyzed in detail the optical properties of the slab in different frequency regions and for different filling fractions and interpreted the results in terms of the macroscopic dielectric function. We have found characteristic features in the response such as reflection and absorption bands the positions and widths of which can be controlled through the filling fraction and the permittivities of the particles and the host medium. These novel optical

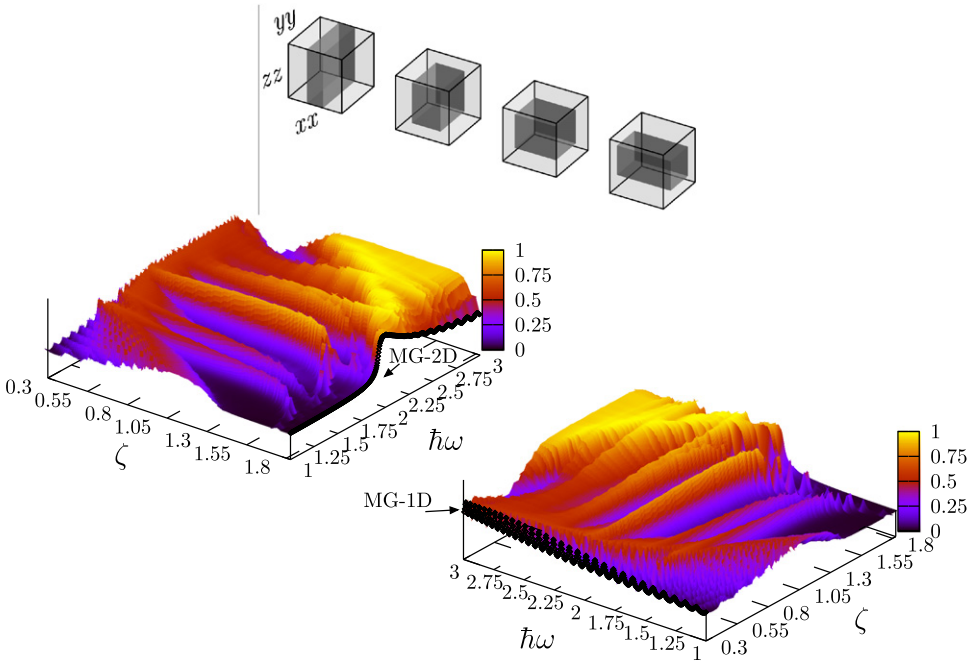

Figure 8. Two views of the absorptance A of a composite slab made of Ag square prisms embedded in a TiO_2 matrix versus their aspect ratio ζ and the photon energy $\hbar\omega$. The slab lies on the xy plane and the light propagates along z and is linearly polarized along x. The filling fraction is fixed at $f = 0.3$. The inset shows the shapes of the particles corresponding to $\zeta \approx 0.3$, 0.7, 1.2 and 1.8. With black lines we show the results of the MG theory in 1D corresponding to $\zeta = 0.3$ and MG in 2D corresponding to $\zeta = 1.8$. The two views are mutually rotated by 90°.

properties are related to the excitation of multipolar resonances of orders higher than the dipolar.

The ENR allowed us to swiftly explore systems with varying geometrical parameters, including such non-trivial geometries as those corresponding to such high filling fractions that neighbor particles interpenetrate and for which other calculation schemes are inapplicable. We further illustrated the versatility of the ENR formalism by calculating the optical properties of an array of prisms of varying aspect ratio interpolating continuously between a 1D superlattice, a 3D cubic array of cubes, and a 2D square array of wires.

It is worth mentioning that although the faceted shape of the discretized particles is a drawback for modeling spherical inclusions, it can also be viewed as an advantage for studying the optical features of synthesized metallic nanoparticles that exhibit facets as a consequence of the manufacturing process [43–45]. The ENR therefore constitutes a versatile tool to investigate and design the optical properties of metallic nanoparticle composites.

Acknowledgements

This work was supported by Agencia Nacional de Promoción Científica y Tecnológica (FONCYT-UNNE PICT-PRH-135-2008 (G.O.)), Consejo Nacional de Investigaciones Científicas y Técnicas (PIP 112-200801-01880 (R.D., D.S. and M. I.)), Universidad de Buenos Aires (UBA-20020100100533 (D.S. and M.I.), and (UBA-20020100100327 (R.D.)), and Universidad Nacional Autnoma de Mxico (DGAPA-IN108413 (W.L.M.)).

References

[1] Bergman D J 1976 Calculation of bounds for some average bulk properties of composite materials *Phys. Rev.* B **14** 4304–12

[2] Fuchs R 1977 Optical properties of small-particle composites *Electrical Transport and Optical Properties of Inhomogeneous Media* (*AIP Conference Proceeding* number 40) ed J C Garland and D B Tanner (American Institute of Physics) pp 276–81

[3] Milton G W 1980 Bounds on the complex dielectric constant of a composite material *Appl. Phys. Lett.* **37** 300–2

[4] Mochán W L and Barrera R G 1985 Electromagnetic response of systems with spatial fluctuations. i. general formalism *Phys. Rev.* B **32** 4984–8

[5] Mochán W L and Barrera R G 1985 Electromagnetic response of systems with spatial fluctuations. ii. applications *Phys. Rev.* B **32** 4989–5001

[6] Barrera R G, Monsivais G M and Mochán W L 1988 Renormalized polarizability in the Maxwell–Garnett theory *Phys. Rev.* B **38** 5371–9

[7] Ghosh K and Fuchs R 1991 Critical behavior in the dielectric properties of random self-similar composites *Phys. Rev.* B **44** 7330–43

[8] Felderhof B U, Ford G W and Cohen E G D 1982 Cluster expansion for the dielectric constant of a polarizable suspension *J. Stat. Phys.* **28** 135–64

[9] Barrera R G, Monsivais G M, Mochán W L and Anda E 1989 Diagrammatic approach to the effective dielectric response of composites *Phys. Rev.* B **39** 9998–10008

[10] Garland J C and Tanner D B (ed) 1978 *Electrical Transport and Optical Properties of Inhomogeneous Media* (*AIP Conference Proceeding No. 40*) (New York: American Institute of Physics)

[11] Mochán W L and Barrera R G (ed) 1994 *Electrical Transport and Optical Properties of Inhomogeneous Media* (*Physica A 207, Num 1–3*) (The Netherlands: Elsevier)

[12] Shalaev V M 1996 Electromagnetic properties of small-particle composites *Phys. Rep.* **272** 61–137
[13] Milton G W, Golden K M, Dobson D and Vardeny A Z (ed) 2003 *Electrical Transport and Optical Properties of Inhomogeneous Media* (*Physica B 338, Num 1–4*) (North-Holland: Elsevier)
[14] Ortiz G P, Martínez-Zérega B E, Mendoza B S and Mochán W L 2009 Effective optical response of metamaterials *Phys. Rev.* B **79** 245132
[15] Cortes E, Mochán W L, Mendoza B S and Ortiz G P 2010 Optical properties of nanostructured metamaterials *Phys. Status Solidi* B **247** 2102–7
[16] Mochán W L, Ortiz G P and Mendoza B S 2010 Efficient homogenization procedure for the calculation of optical properties of 3D nanostructured composites *Opt. Express* **18** 22119–27
[17] Mendoza B S and Mochán W L 2012 Birefringent nanostructured metamaterials *Phys. Rev.* B **85** 125418
[18] Bruggeman D A G 1935 Berechnung verschiedener physikalischer konstanten von heterogenen substanzen. i. dielektrizitätskonstanten und leitfähigkeiten der mischkörper aus isotropen substanzen *Ann. Phys.* **416** 665–79
[19] Maxwell-Garnett J C 1904 Colours in metal glasses and metal films *Philos. Trans. R. Soc. London* A **203** 385–420
[20] Waterman P C and Pedersen N E 1986 Electromagnetic scattering by periodic array of particles *J. Appl. Phys.* **59** 2609–18
[21] Doyle W T 1977 The permitivity of cubic arrays of spheres *Electrical Transport and Optical Properties of Inhomogeneous Media* (*AIP Conference Proceeding* number 40) ed J C Garland and D B Tanner (American Institute of Physics) p 300
[22] Claro F 1984 Theory of resonant modes in particulate matter *Phys. Rev.* B **30** 4989
[23] Yannopapas V and Moroz A 2005 Negative refractive index metamaterials from inherently non-magnetic materials for deep infrared to terahertz frequency ranges *J. Phys.: Condens. Matter* **17** 3717–34
[24] Moroz A 2009 Localized resonances of composite particles *J. Phys. Chem. C.* **113** 21604–10
[25] Chern R L and Liu X X 2010 Effective parameters and quasi-static resonances for periodic array of dielectric spheres *J. Opt. Soc. Am.* B **27** 488–96
[26] Barrera R G and Mendoza C I 1994 Three-particle correlations in the optical properties of granular composites *Solar Energy Materials and Solar Cells* **32** 463
[27] Ortiz G P, López-Bastidas C, Maytorena J A and Mochán W L 2003 Bulk response of composite from finite samples *Physica* B **338** 54–57
[28] Rojas R and Claro F 1986 Electromagnetic response of an array of particles: normal-mode theory *Phys. Rev.* B **34** 3730
[29] Geist B, Spillman W B Jr and Claus R O 2005 Thermal cycling and the optical and electrical characterization of self-assembled multilayer nile blue a-gold thin films *Appl. Opt.* **44** 6357–60
[30] Lee J H, Wu Q and Park W 2009 Metal nanocluster metamaterial fabricated by the colloidal self-assembly *Opt. Lett.* **34** 443–5
[31] Mühlig S, Rockstuhl C, Yannopapas V, Bürgi T, Shalkevich N and Lederer F 2011 Optical properties of a fabricated self-assembled bottom-up bulk metamaterial *Opt. Express* **19** 9607–16
[32] Modinos A 1987 Scattering of electromagnetic waves by a plane of spheres-formalism *Physica* A **141** 575–88
[33] Stefanou N, Yannopapas V and Modinos A 1998 Heterostructures of photonic crystals: frequency bands and transmission coefficients *Comput. Phys. Commun.* **113** 49–77
[34] Yannopapas V, Modinos A and Stefanou N 1999 Optical properties of metallodielectric photonic crystals *Phys. Rev.* B **60** 5359
[35] Stefanou N, Yannopapas V and Modinos A 2000 Multem 2: a new version of the program for transmission and band-structure calculations of photonic crystals *Comput. Phys. Commun.* **132** 189–96
[36] Dorado L A, Depine R A and Míguez H 2007 Effect of extinction on the high-energy optical response of photonic crystals *Phys. Rev.* B **75** 241101
[37] Haydock R 1980 The recursive solution of the Schrödinger equation *Solid State Physics* **35** 215
[38] Glazebrook K, Brinchmann J, Cerney J, DeForest C, Hunt D, Jenness T, Luka T, Schwebel R and Soeller C 1997 *Pdl: The Perl Data Language V.2.4.4* Dr. Dobb's Journal http://pdl.perl.org
[39] Johnson P B and Christy R M 1972 Optical constant of noble metals *Phys. Rev.* B **6** 4370
[40] Kreibig U and Vollmer M 1995 *Optical Properties of Metal Cluster* (Berlin: Springer)
[41] Ghenuche P, Vincent G, Laroche M, Bardou N, Haïdar R, Pelouard J-L and Collin S 2012 Optical extinction in a single layer of nanorods *Phys. Rev. Lett.* **109** 143903
[42] Fuchs R 1975 Theory of the optical properties of ionic crystal cubes *Phys. Rev.* B **11** 1732
[43] Wang Z L 2000 Transmission electron microscopy of shape-controlled nanocrystals and their assemblies *J. Phys. Chem. B.* **104** 1153
[44] Yacaman M J, Ascencio J A, Liu H B and Gardea-Torresdey J 2001 Structure shape and stability of nanometric sized particles *J. Vac. Sci. Technol. B.* **19** 1091
[45] Gonzalez A L, Noguez C, Ortiz G P and Rodriguez-Gattorno G 2005 Optical absorbance of colloidal suspensions of silver polyhedral nanoparticles *J. Phys. Chem.* B **109** 17512–7